Collective Phonon-Polaritonic Modes in SiC Subarrays

Guanyu Lu[1], Christopher R. Gubbin[2], J. Ryan Nolen[3], Thomas Folland[4], Katja Diaz-Granados[3], Ivan I. Kravchenko[5], Joseph Spencer[6], Marko J. Tadjer[6], Orest. J. Glembocki[1], Simone De Liberato[2], Joshua D. Caldwell[1]

1. Department of Mechanical Engineering, Vanderbilt University, Nashville, Tennessee 37212, United States

2. School of Physics and Astronomy, University of Southampton, Southampton SO17 1BJ, United Kingdom

3. Interdisciplinary Materials Science, Vanderbilt University, Nashville, Tennessee 37212, United States

4. School of Physics and Astronomy, The University of Iowa, Iowa City, Iowa, 52242, United States

5. Center for Nanophase Materials Sciences, Oak Ridge National Laboratory, Oak Ridge, Tennessee, 37830, United States

6. US Naval Research Laboratory, Washington, Washington, D.C. 20375, United States

Abstract

Localized surface phonon polaritons (LSPhPs) provide an emerging platform to engineer light-matter interactions through nanoscale patterning for a range of mid-infrared application spaces. However, polar material systems studied to date have mainly focused on simple designs featuring a single element in the periodic unit cell. Increasing the complexity of the unit cell can serve to modify the resonant near-fields, intra- and inter-unit-cell coupling, as well as offering pathways to dictate spectral tuning in the far-field. In this work, we exploit more complicated unit-cell structures to realize new LSPhP modes with additional degrees of design freedom, which are largely unexplored. Collectively excited LSPhP modes with distinctly symmetric and anti-symmetric near-fields are supported in these subarray designs, which are based on nanopillars that are scaled by the number of subarray elements to ensure a constant unit cell size. Moreover, we observe an anomalous mode-matching of the collective symmetric mode in our fabricated subarrays that are robust to changing numbers of pillars within the subarrays, as well as to defects intentionally introduced in the form of missing pillars. This work therefore illustrates the hierarchical design of tailored LSPhP resonances and modal near-field profiles simultaneously for a variety of IR applications such as surface-enhanced spectroscopies and biochemical sensing.

Keywords: localized surface phonon polariton, monopolar resonance, unit cell, strong coupling, mid-infrared

Introduction

The sub-diffractional confinement of light can be achieved through the fabrication of sub-wavelength polaritonic structures, which enable the modulation of light-matter interactions through user-designed patterns. Such localized confinement of electromagnetic energy, which is on length-scales that are orders of magnitude shorter than the free space wavelength, find applications in enhanced molecular sensing,[1] nonlinear optics,[2] light generation,[3] and communications.[4] Localized surface phonon polariton (LSPhP) modes provide ideal options to achieve low loss, extreme sub-diffractional photon confinement within the mid-infrared (mid-IR) spectral region,[5-7] which coincides with the molecular fingerprint region of the electromagnetic spectrum and with two atmospheric transmission windows. LSPhPs are induced through light coupling with oscillating ionic charges (optic phonons) within nanostructures fabricated from polar crystals within the material Reststrahlen band. This spectral band is bound by the transverse (TO) and longitudinal optic (LO) phonon frequencies of the polaritonic medium.[8] These excitations possess narrow spectral linewidths due to the long lifetime of optic phonons[9, 10] with the LSPhP resonances able to be tuned through structure design.[3, 10-13] However, while some methods towards active tuning have been reported,[14, 15] direct injection of free carriers remains challenging and induces high losses into the system. Alternatively, the hybridization of LSPhPs with other polaritonic, plasmonic and vibrational modes through strong coupling[16-24] offers a means to obtain such tuning without dramatic increases in loss, providing a wide range of functionalities.[1, 25-31] One example is the hybridization of LSPhPs with propagating modes to engineer the spatial and spectral dispersion of thermal emission.[27] While those objectives can be fulfilled within periodic structures featuring a single repeated (1x1) element in the LSPhP unit cell, as demonstrated in previous studies,[32, 33] there are limitations resulting from such a simple unit cell design. For example, while one can periodically space polar nanostructures at distances on the order of the free-space wavelength of light to induce diffractive coupling between localized and propagating modes,[27] this necessarily reduces the filling fraction and thereby lacks the stronger field enhancements that are observed within coupled polaritonic modes observed within nanoscale gaps between structures.[34] Moreover, for simple unit cell designs a limited range of LSPhP modes are supported, restricting design freedom and the ability to work with more complex sensing applications such as chemical fingerprints. This therefore raises the question: can we modify the LSPhP unit cell to manipulate new polariton properties and enable additional spectral tunability and near-field pattern design?

By increasing the complexity of the unit cell for subwavelength polaritonic structures, new polaritonic resonant properties can potentially be engineered. Similar to atoms in different arrangements forming molecules,[35] interacting nanostructures in metallic complexes, such as dimers,[36-38] trimers,[39] quadrumers,[39, 40] can give rise to collective modes, enabling the design of resonant properties. More importantly, the polaritonic response of these collectively excited polaritonic modes greatly depends on the spatial arrangement of the nanostructures[41-46] as well as the intrinsic optical properties of individual elements.[47] Similarly, to design new LSPhP resonant properties, more repeatable elements can be added into the unit cell of the polar nanostructures (Fig. 1a), for example, 2x2, 3x3, 4x4 subarrays of nanopillars as the unit cell basis. Such unit cells are especially interesting for sensing applications as altering the composition and subarray structure could allow for additional polaritonic resonances, enhanced spectral tuning, improved definition of the local near-fields and offer greater control of the field enhancement and distribution. Further, subarray designs offer the potential to design the localized modes much like controlling the unit cell in a crystal, while still allowing for unit cell periodicities to be employed for

exploiting diffractive coupling to induce spatial coherence.[27, 48] However, the polaritonic properties for the LSPhP system with increasing unit cell complexity remain largely unexplored.

In this work, we explore subarray designs of subwavelength nanopillars etched into semi-insulating 4H-SiC substrates, which can support low-loss, LSPhP modes with collective behaviors. In the subarray design, the unit cell (1x1, 2x2, 3x3, 4x4) is maintained at a constant size and periodicity, inferring that the pillars comprising the subarrays are scaled to smaller sizes based on the number of elements in the subarray (*e.g.* pillars in 2x2 are 50% of the diameter for the 1x1 architecture). By introducing more complex unit cells, excitation of collective LSPhP modes resulting from near-field interactions between neighboring elements are observed in our far-field measurements, electromagnetic simulations, and *via* a tight-binding theoretical model. Referring to the terminology for the electromagnetic analog of molecular orbital theory in coupled plasmonic systems,[34, 35] we report on the observation of collective symmetric and anti-symmetric modes supported within LSPhP subarrays featuring 2x2 to 4x4 collections of pillars with respect to the simple 1x1 architecture explored in prior works.[9, 11, 25] When the subarray is formed, these new symmetric and anti-symmetric LSPhPs modes split around the frequency of the original mode supported by the single resonant antenna in the 1x1 unit cell (Fig. 1a, green and blue). Yet, interestingly, we observe a quasi-mode-matching of the collective symmetric mode within our subarray designs whereby the frequency of the resonance is found to be nominally independent of the number of pillars in the subarray (Fig. 1a, blue and red). In addition, the anti-symmetric mode is found to be primarily dictated by the near-field interactions within the unit cell, possessing higher polariton confinement. In contrast, the symmetric mode is observed as an extended excitation with long range interactions between adjacent unit cells, akin to the monopolar resonance described in previous works.[9, 11, 49, 50] Moreover, these previously unexplored collective LSPhP modes are found to be robust to defects introduced into the unit cell (*e.g.* removal of certain pillars within the subarray), opening up possibilities for symmetry-protected states in such collective LSPhP modes. As such, our subarrays described here represents a modal design platform that offers the low-loss, subdiffractional confinement of light associated with LSPhPs, but expanding the precise spectral tuning of the electromagnetic resonances, near-field distributions and potential to be hybridized with other resonances resulting from the subarray architecture.

Results

In order to explore the polaritonic properties introduced by LSPhP resonator unit cells with increased complexity, we begin by scaling a unit cell featuring a single nanopillar (1x1 unit cell) to a 2x2 design, maintaining a constant unit cell size, *e.g.*, for a 1x1 pillar subarray diameter of 2 μm, the pillar diameter used in the 2x2 unit cell is 1 μm. In all cases the pillar height (1 μm) was maintained. While several unit cell periodicities were explored, for initial comparisons we consider a group of matched structures where the periodicity was set to a fixed value of 6 μm. For completeness, the 2x2 structure is also compared to a 1x1 structure with the same pillar diameter (1 μm). The schematics of the corresponding unit cells are provided in Fig. 1a. The nanopillars are fabricated into a semi-insulating 4H-SiC substrate using standard electron beam lithography (EBL) and reactive ion etching (RIE) processes (details in methods, with SEM images of the fabricated structures provided in SI). Due to the sloped sidewall of the pillars introduced by the RIE (about 82 degrees), we define the gap within the multiple pillar unit cells as the edge-to-edge distance between the tops of the pillars, which is about 300 nm for the fabricated 2x2 structures discussed initially. By measuring the far-field reflection spectra of the fabricated structures (methods), collective behaviors of the LSPhP resonances in subarrays can be probed. Two types of LSPhP modes were identified

in previous studies of simple 1x1 structure.[9, 11, 50, 51] The first is the monopole resonance that results from a modified longitudinal dipole where a uniform near-field charge distributed along the height of the pillar is balanced by an opposing phase on the surface of the substrate between adjacent structures. This mode can be excited when the impinging electric field has a component orientated perpendicular to the substrate plane, as in off-normal incidence, *p*-polarized excitation.[9, 11, 51] The second, which occurs at higher energies, is the transverse dipole resonance. This mode can be excited when the impinging electric field has a component parallel to the substrate plane. For the out-of-plane excitation (oblique illumination), both *p*- and *s*-polarized illumination result in the observation of this mode. In this work, the monopole mode is of primary interest, as it supports longer range interactions and usually exhibits a higher quality factor (Q-factor).[9, 11] Thus, for this study we maintained the 100 nm Ni hard mask on top of the 4H-SiC nanopillars (from nanofabrication) in an effort to suppress the excitation of the first transverse dipole resonance, while maintaining strong in-coupling to the monopole mode.[11]

By comparing the experimental reflection spectra of different fabricated structures, we can explore the different LSPhP modes that are supported. To simplify the discussion we begin by comparing the 2x2 with the 1x1 structures that have the same pillar diameter of 1 μm (Fig. 1b, blue and green). For the 1x1 structure, the monopolar resonance is observed at 849 cm^{-1} and agrees well with previous studies.[9, 11] In addition, a second weak reflection dip at 838 cm^{-1} is identified that corresponds to the zone-folded LO (ZFLO) phonon mode associated with the 4H-SiC polytype.[52] By extending the 1x1 to the 2x2 subarray architecture, the monopole mode is observed to split into two resonances centered about the frequency of the 1x1 monopolar mode, with one at a higher frequency at 866 cm^{-1}, while the other emerges at 825 cm^{-1} below the ZFLO mode. Yet, if the diameter of the nanopillars in the 2x2 array are halved such that the total unit cell size is maintained to that of the 1x1 structures (e.g. the 1x1 diameter is double that of the individual pillars within the 2x2 subarrays; Fig. 1b, red and blue), the higher frequency resonance is maintained at approximately the same resonant frequency with a similar absorption amplitude as for the 1x1 monopole mode (864 cm^{-1}), while another lower frequency mode emerges that is not found in the 1x1 structure. The 2x2 LSPhP modes therefore offer a glimpse into the design flexibilities that such a subarray design approach can offer in dictating the resultant polariton properties.

To further understand the origin of these modes we performed finite element method (FEM) simulations of the fabricated structures using CST studio (methods). The simulated unpolarized reflection spectra (Fig. 1c) agree well with our experimental measurements (Fig. 1b) with only slight deviations in the spectral positions of the modes (polarized spectra are provided in SI). The simulated electric field (E_z) of the 1x1 monopole resonance indeed reveals itself as the anticipated modified longitudinal dipole with the modal symmetry across the resonator featuring strong inter-unit-cell coupling (Fig. 1d and Fig. 1g). The higher energy monopole resonance observed from the 2x2 structure (Fig. 1f) exhibits an almost identical electric field distribution when matching the unit cell size to that of the 1x1 structure (Fig. 1g) and similarly can only be excited by *p*-polarized light (Fig. S2 in the SI). Thus, we can identify this 2x2 localized mode as a collective monopolar resonance, which is excited by the near-field interaction between neighboring elements in the unit cell. Since all the neighboring nanopillars exhibit the same phase at the top of the structures, we term this collectively excited mode as the symmetric (S) monopolar mode. This implies that the small gap between pillars in the subarray hosts the overlapping evanescent fields between the adjacent pillars, which will result in the effective lateral dimensions of the nanopillars being increased, thereby resulting in a slight blue shift in the spectral position (Fig. 1b and Fig. 1c, red and blue) as expected with increasing pillar diameter.[50] On the contrary, the electric field distribution of the newly emerged 2x2

narrowband resonance at lower energy exhibits opposite phases on neighboring pillars and is strongly confined to the individual subarray with almost no net dipole moment in the unit cell (Fig. 1e). This mode can still couple to the far field as the out-of-plane polarization is uniform along the wavefront of the illumination beam, albeit with reduced in-coupling compared to the symmetric mode. Thus, we refer to this as the anti-symmetric (A) monopolar mode. The emergence of the S and A modes in the 2x2 structure is anticipated by the electromagnetic simulations and can be explained using a concept analogous to the plasmon hybridization reported in plasmonic dimers.[34, 53] By employing a tight-binding model (methods), we also confirm that when the subarray is formed in the phonon polariton system, the original 1x1 monopole mode splits into new symmetric and anti-symmetric superpositions, with distinct light confinement for the two new modes. Although all the measurements in the manuscript are taken at 25° incident angle, we also investigate the S and A modes at normal incidence where only the A mode can be supported while the S mode cannot be excited (Fig. S3). These collectively excited modes also raise an obvious question: what is the influence of the spatial arrangement of the elements in the subarray upon the resonant properties and near-field distributions?

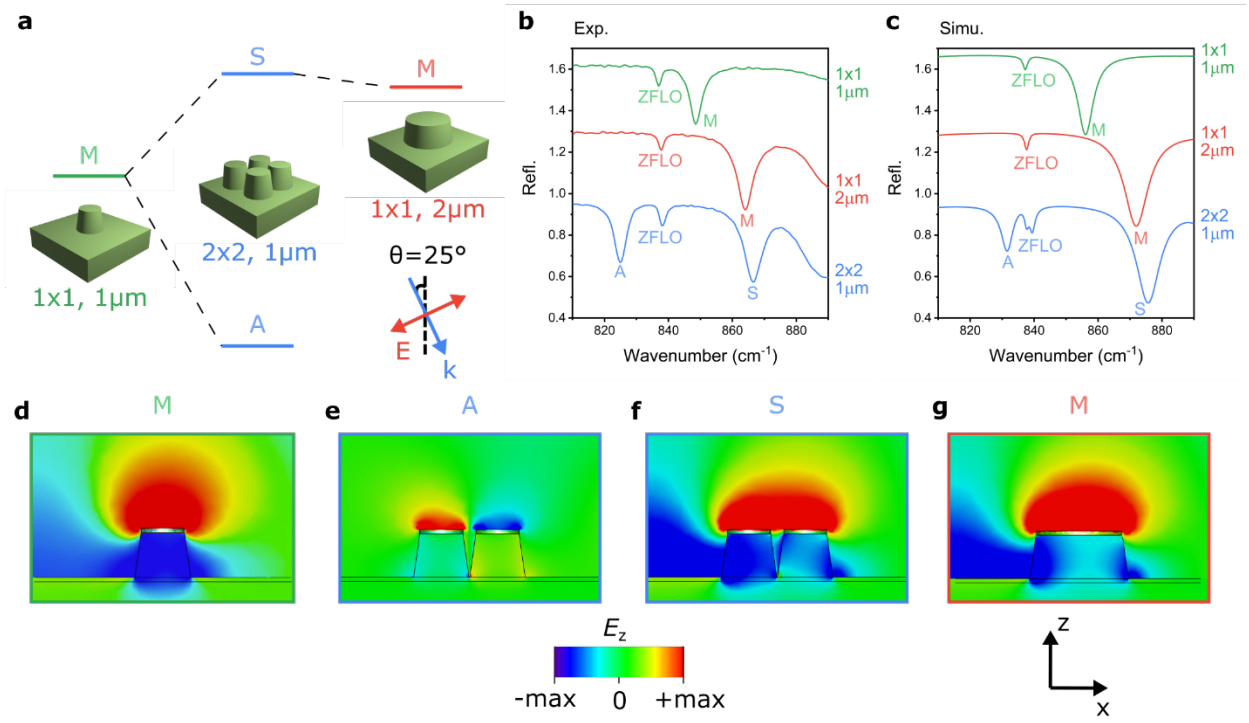

Figure 1: The symmetric and antisymmetric monopole modes in SiC subarray. (a) Level diagram for the collectively excited monopole modes. M: bare monopole mode; A: anti-symmetric monopole mode; S: symmetric monopole mode. (b) Experimental unpolarized reflection spectra for the 1x1 and 2x2 nanostructures with the same unit cell period (6 μm) and nanopillar height (1 μm). For 1x1, the diameters of the nanopillars are 1 μm (green) and 2 μm (red), and for 2x2, the diameter of the nanopillars is 1 μm with a 300 nm gap in the unit cell (blue). (c) Simulated reflection spectra (average of *p*- and *s*-polarized spectra to mimic the unpolarized light used in the experiments) for the 1x1 and 2x2 nanostructures with the same geometries in (b). The reflection spectra in (b) and (c) are shifted by 0.35 for clarity. Simulated field (E_z) of the modes in (c): bare monopole mode for 1x1 structure with 1 μm diameter (d); Anti-symmetric mode for 2x2 structure with 1 μm diameter (e); Symmetric mode for 2x2 structure with 1 μm diameter (f); bare monopole mode for 1x1 structure with 2 μm diameter (g). The scale bar is the same for the simulated fields in (d)-(g).

To further understand the polariton properties within our subarray platform, we studied how the geometries of the structures within the 2x2 unit cell dictate the spectral tuning of the S and A modes. We

therefore examined the impact of the interpillar gap within the 2x2 subarray while maintaining the nanopillar diameter and periodicity of the unit cell of the fabricated structure in Fig. 1. By plotting the experimental reflection spectra of the structures featuring different gaps into a contour plot, we can track the dispersion of the collectively excited modes (Fig. 2a). From these dispersion plots a clear blue shift of the A mode toward the ZFLO with increasing gap size is observed. With further increased gap these modes become coupled, resulting in a hybridization between the A and ZFLO modes.[26] Further, as the lower A branch shifts to lower frequencies below that of the ZFLO, another polariton emerges to the high frequency side as a result of strong coupling between these two modes. However, as the interpillar gap continues to grow, the absorption amplitude of this mode is reduced (this is more visible using a different color scale in the contour plot featuring only the A mode, which is presented in Fig. S4a). For the A mode, the interpillar coupling within the subarray is weak as the electric field is confined within the nanopillars (Fig. 1e). The coupling between the A mode and the ZFLO can also be determined by the comparison with simulated structures made of 3C-SiC, where the isotropic crystal structure precludes the presence of the ZFLO phonon(s) (see Fig. S4 in the SI). The gap dependence of the A mode can be explained using electromagnetic hybridization theory by referring to its near-field energy distribution (Fig. 1e). The Coulomb attraction between the fields supported on neighboring pillars in the unit cell will increase with decreasing gap. This in turn will lead to a reduction in the energy of the A mode and confirms it as a collectively excited resonance inside the unit cell. In contrast, the S mode only slightly blue-shifts (about 1 cm^{-1}), exhibiting almost the same resonant frequency as the 1x1 monopole mode in Fig. 1b (red). This is due to its long-range interactions with adjacent unit cells that dominates its behavior over the interpillar coupling within the unit cell. By extracting the spectral position of the reflection dips in the experimental dispersion plot we can track the measured absorption amplitude with increasing gap (Fig. 2b). Here, absorption is defined as 1 – reflection, as there is no transmission inside the Reststrahlen band of 4H-SiC, and scattering is ignored. There is a slight decrease in absorption for the S mode when increasing the gap, with its amplitude approaching 0.5 under the unpolarized illumination, which implies near-unity absorption of *p*-polarized light. As for the A mode, the absorption amplitude drops significantly as the gap inside the unit cell increases due to the reduction in interpillar coupling.

The linewidths of the collective modes can also be extracted by performing Lorentzian line-shape fitting of the experimental spectra (Fig. 2c). The FWHM (full width at half maximum) of the S mode remains consistent as the gap is increased, yielding a Q-factor ranging from 136 to 148. This range is consistent with that of the 1x1 structure with a 2 μm diameter (148; Fig. 1b). For the A mode, the FWHM at small gaps is comparable to that of the S resonance, however, a dramatic reduction in the linewidth results as the resonance shifts towards and couples to the ZFLO mode. The coupling to the extremely narrow ZFLO mode that occurs upon increasing the gap greatly enhances the Q-factor of the hybrid ZFLO/A mode, which is shown to approach 500. Even though we are limited by the resolution of our spectrometer (2 cm^{-1}), this Q-factor is comparable with the record-high far-field Q-factor (501) recently reported,[54] however, we reiterate that this is the result of strong coupling and not indicative of the inherent linewidth of the uncoupled A mode.

As demonstrated above, the interpillar gap plays a strong role in dictating the spectral dispersion of the A mode, while having a limited impact upon the S resonance, however, the role of the nanopillar diameter within a subarray unit must also be understood. As the diameter is a principal parameter driving the resonant frequency of both the A and S modes, here we explore the diameter dependence of the polaritonic dispersion to investigate the behavior of the S (A) resonance as it spectrally approaches (moves

away from) the ZFLO. Keeping the interpillar gap (300 nm) and other geometric parameters the same as the fabricated 2x2 structure in Fig. 1, we plot the experimental reflection spectra as a dispersion plot in Fig. 2d. Both modes are found to redshift with decreasing pillar diameter, with the S mode approaching the ZFLO at smaller diameters, giving rise to an anti-crossing similar to what was observed for the A mode above. This in turn results in the formation of an upper (UB) and lower branch (LB), which is a hallmark of polaritonic strong coupling.[16-18, 25-27] On the contrary, the spectral overlap of the A with the ZFLO is reduced, resulting in the ability to quantify the behavior of this resonance without the complications of the strong coupling effects. The absorption amplitudes of the S(UB) and A branches are both shown to decrease with decreasing nanopillar diameter (Fig. 2e), consistent with the reduction in surface area. The higher absorption amplitude of the S mode in comparison to the A resonance also suggests that the former is more accessible from the far-field as predicted based by its near-field distribution. However, the A mode consistently exhibits a narrower linewidth (Fig. 2f) even in the absence of strong coupling with the ZFLO phonon, thus providing a higher Q-factor than the uncoupled S mode (uncoupled Q=208 for A mode and Q=148 for S mode). The behavior of the collectively excited S and A modes with decreasing pillar diameter is analogous to the red shifting of the individual monopole resonances supported by a 1x1 structure,[9, 11, 50] implying further that the subarray resonances offer a mechanism towards achieving an anomalous mode matching between the individual and subarray nanopillar architectures.

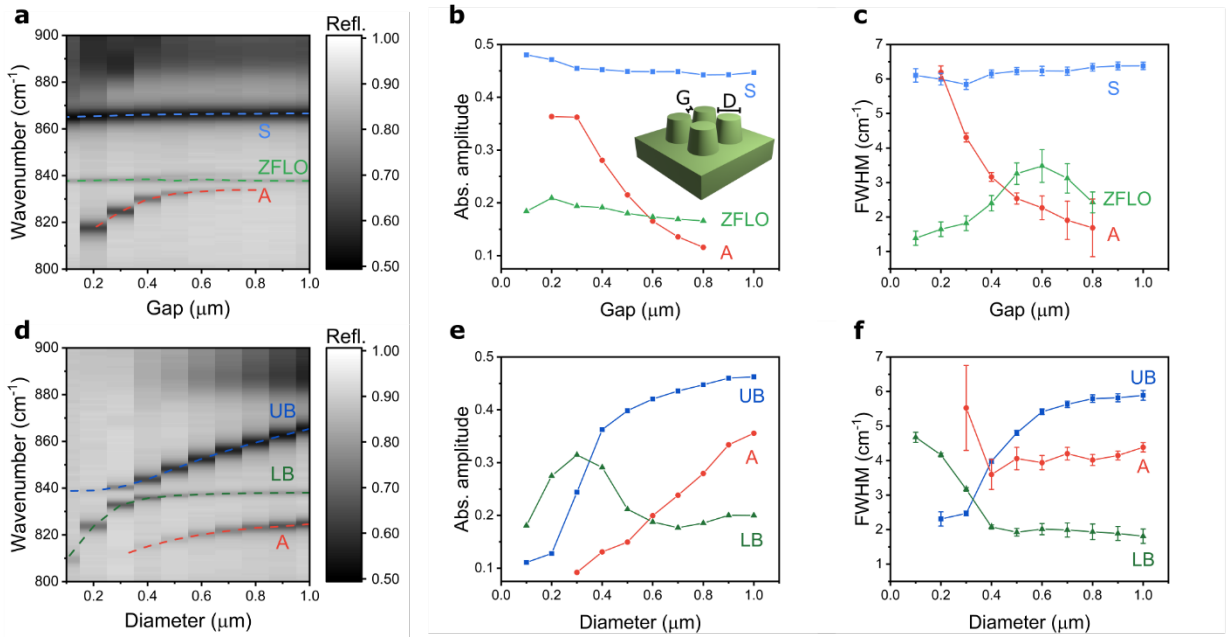

Figure 2: Tuning of the symmetric and antisymmetric modes in 2x2 subarray. Experimental dispersion plot made of reflection spectra for 2x2 structure with different gaps in the unit cell (a) and different nanopillar diameters (d). Peak positions from Lorentz fitting of the experimental spectra are plotted on top of the dispersion plots in (a) and (d) to better illustrate. Absorption amplitude of the investigated modes for 2x2 structure with different gaps in the unit cell (b) and different pillar diameters (e). Linewidth (FWHM) of the investigated modes for 2x2 structure with different gaps in the unit cell (c) and different pillar diameters (f). Inset in (b) illustrates the tuning parameters (gap: G and diameter: D). The error bars in (c) and (f) are the uncertainty from the Lorentz fitting of the reflection dips. For the 2x2 structure with different gaps, the period of the unit cell is 6 μm and the pillar diameter is 1 μm. For the 2x2 structure with different diameters, the period of the unit cell is 6 um and the gap in the unit cell is 0.3 μm.

To further investigate the anomalous mode matching of these collectively excited modes, we extended this subarray concept from 2x2 to 3x3 and 4x4 unit cells, again maintaining a constant unit cell size, with

subarrays featuring pillars that are scaled to smaller sizes based on the number of elements (Fig. 3 a-d) as discussed previously. Maintaining the interpillar gap at 300-nm for each subarray, we explore the role of the unit cell periodicity to examine the experimental dispersion of the collective modes (Fig. 3a-d) as a function of subarray structure. Again, we observe the expected redshift in the monopole resonance for the 1x1 structure (Fig. 3a, M), as increasing the period translates into a reduced interpillar coupling. Similarly, the 2x2, 3x3, 4x4 S modes (Fig. 3b-d, S) follow an almost identical dispersion. Thus, despite the dramatic difference in unit cell geometry, the anomalous mode matching of the S mode is maintained, illustrating the generalized nature of this effect.

Finally, to test the robustness of the resonant S and A modes to the presence of defects in the subarray design, we fabricated similar subarray structures, but with some of the pillars removed. In addition to the square subarray designs discussed above, we also patterned a 3x3 structure missing the center pillar (Fig. 3e), an 'X-shape' (Fig. 3f), and a 'cross-shape' (Fig. 3g), as well as a related 4x4 structure without the center pillars (Fig. 3h). In all cases a similar dispersion of the S mode is reported, thereby illustrating the remarkable robustness of the far-field resonances to changes in the subarray structure. However, the non-dispersive A mode was found to be substantially stronger in square subarrays (Fig. 3 b-d, A) than in those where defects are present (Fig. 3e-h, A). Additionally, we note that two A modes emerge in structures with broken symmetry for the 3x3 structure (Fig. 3e, A_1 and A_2). Yet, neither shifts appreciably over the range of periods probed as they are more strongly confined to the individual subarrays and thus, do not exhibit significant evanescent extension over the substrate surface between subarrays. On the other hand, the magnitude of the frequency shifts of the S mode increased with an increasing number of pillars in the square subarray (Fig. 3 a-d). This could be attributed to the increased charge density at the array edge as the number of pillars grows. Smaller frequency shifts are reported for the cross and X-shape arrays (Fig. 3f and Fig. 3g), which we attribute to the removal of pillars from the array edges, thereby decreasing the coupling between subarrays. However, despite these small variations, these results imply that a significantly expanded set of design principles can be realized to dictate the near-field patterns without substantially modifying the far-field spectrum.

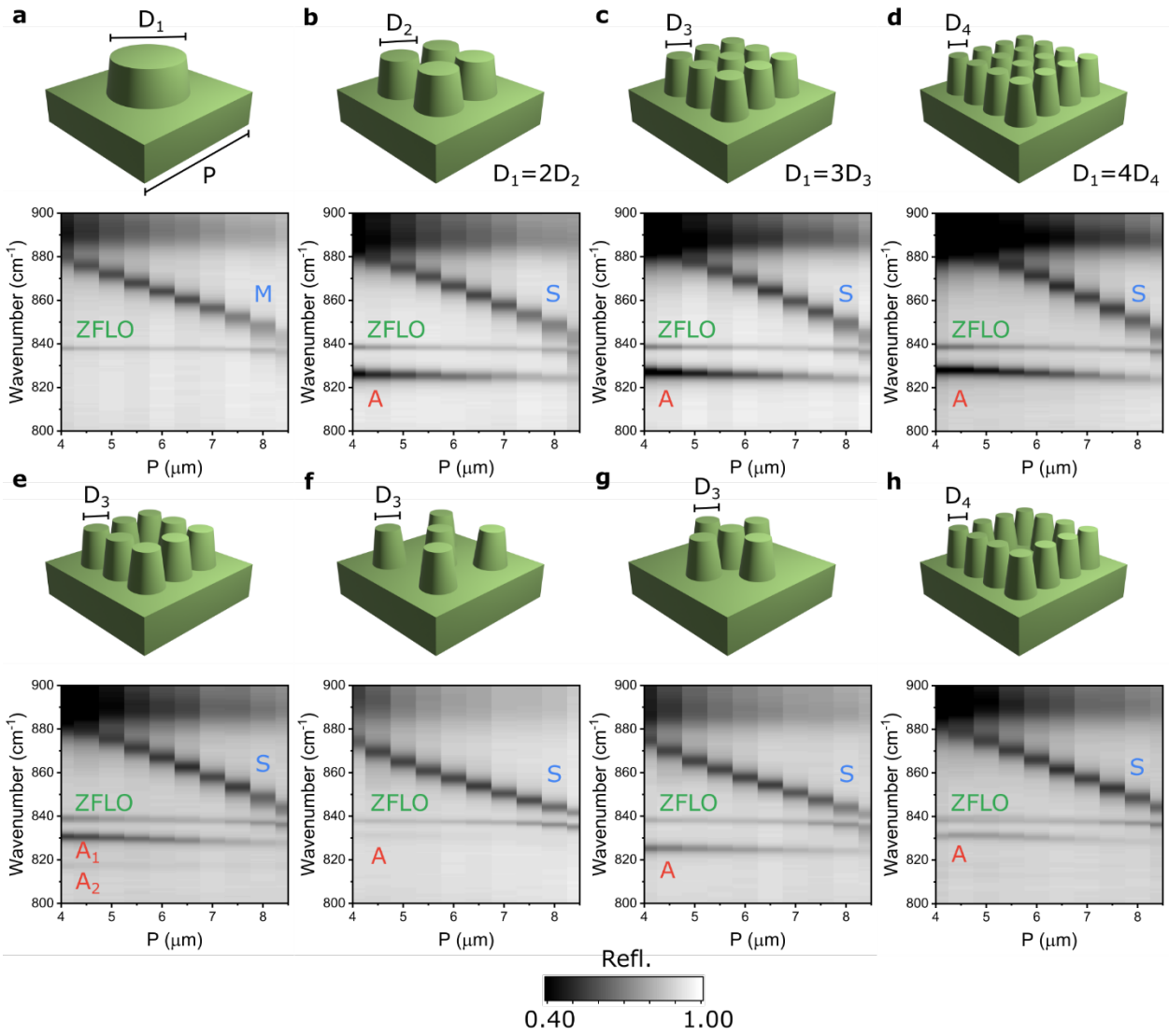

Figure 3: The experimental dispersions of symmetric and antisymmetric modes in the complex subarrays. Experimental dispersion plots made of reflection spectra with different unit cell periods for (a) 1x1 structure, (b) 2x2 structure, (c) square 3x3 structure, (d) square 4x4 structure, (e) 3x3 structure without the center pillar, (f) 3x3 structure features as X-shape, (g) 3x3 structure features as cross-shape, (h) 4x4 structure without center 2x2 pillars.

To quantitatively study the quasi-mode-matching of the S and A modes in these complex subarrays, Lorentz fitting of the experimental spectra is used to extract the modal information from the reflection spectra. As an example, the extracted values for all patterns with the same unit cell period (7 μm) are plotted in Fig. 4. For the square subarrays a consistent blue shift of the collective S mode is observed when increasing the number of pillars in the subarray (dashed blue line in Fig. 4a), which is a result of multiple effects. First, as the pillar diameter is decreased, the bare monopole mode red shifts. The S mode is blue shifted from this bare monopole frequency (1x1 resonant condition) partially compensating the diameter-induced red-shift, although this shift is reduced in arrays containing more pillars. Secondly, as discussed above and in our theoretical model (methods), there is an increased interaction between adjacent subarrays when it contains more pillars as more charge resides at the edges of the subarray. Introducing defects into the unit cell results in a red shift of the frequency of the collective mode (Fig. 4a). This again

is a result of two things. First, as there are less pillars in the array, the blue shift of the S mode from the bare monopole frequency is reduced. Second, for the cross and X-shape arrays, there is less repulsion between adjacent subarrays. As for the absorption amplitude of the S mode, we observe that it increases with increasing number of pillars (Fig. 4b). Interestingly, we identified a similar Q-factor for the S mode of all our fabricated structures independent of diameter or gap, however, it is enhanced with the introduction of defects (Fig. 4c). This could be explained by reference to previous studies of single pillars, where the quality factor was observed to increase with decreasing end facet dimension.[50] As for the A mode, the resonant frequency remains consistent for the square subarrays and independent of the number of pillars, while the presence of defects in the unit cell modifies the resonance frequency, as observed for the symmetric mode (Fig. 4d). The absorption amplitude also increases with pillar number for the square arrays (Fig. 4e), while the presence of defects results in a decrease in the absorption. As for the Q-factor of the A mode, the presence of defects in the unit cell resulted in an enhancement, albeit with the exception of the lower energy mode (A_2) of the 3x3 structure that is missing the center pillar (Fig. 4f).

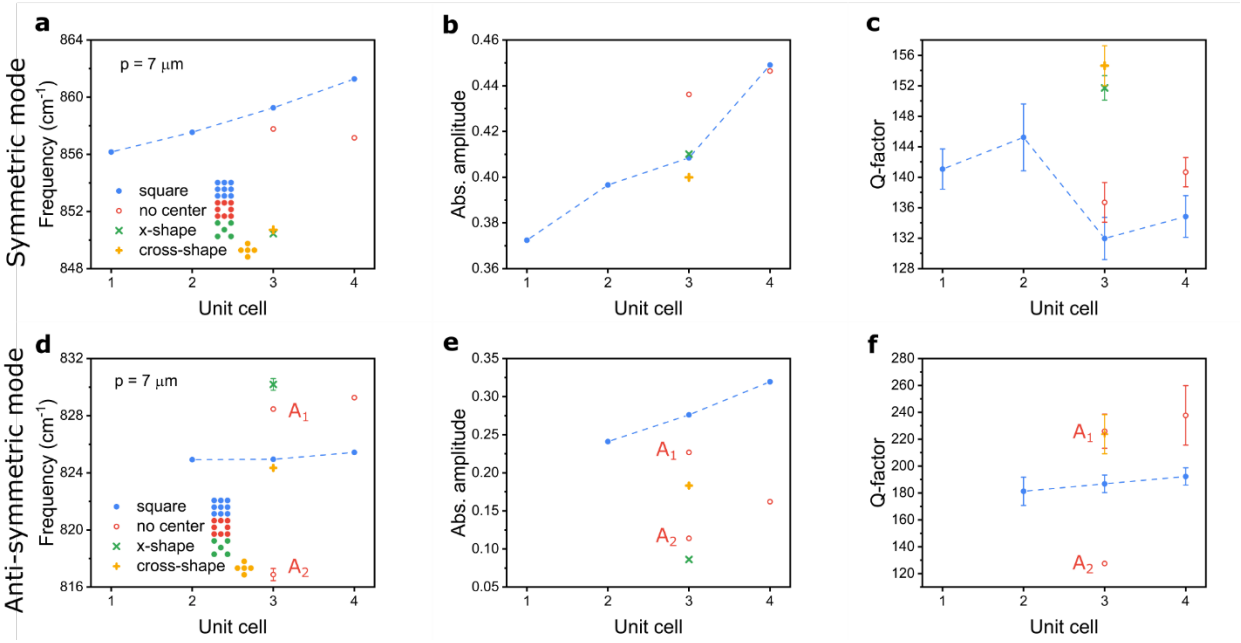

Figure 4: The comparison of symmetric and antisymmetric monopole modes in complex subarrays. Peak positions of the symmetric (a) and anti-symmetric (d) modes for fabricated structure in Fig. 3. Absorption amplitude of the symmetric (b) and anti-symmetric (e) modes for the fabricated structure in Fig. 3. Q-factor of the symmetric (c) and anti-symmetric (f) modes for fabricated structure in Fig. 3. All the results are extracted from the Lorentz fitting of the spectra for the structure with a 7 μm period. Note there are two anti-symmetric modes in the 3x3 structure without center pillar (A_1 and A_2), and Q-factor for the anti-symmetric mode of the 3x3 structure featuring X-shape is not plotted in (f) because the mode is weak with a large error bar.

To further understand the influence of defects on the subarray, we calculated the field distributions of the eigenmodes supported (methods), using the 3x3 structure as an example (Fig. 5). We can categorize the modes of the subarrays into three subsets based on the symmetry of the out-of-plane electric field (E_z) with respect to the two symmetric axes of each resonator array. For the S modes, the out-of-plane field is polarized in the same direction in each quadrant, and these modes are indicated in panels a-k of Fig. 5. The first S mode exhibits fields that are polarized symmetrically (Fig. 5a-d), akin to the monopolar (M) resonance in the simple 1x1 system.[9, 11, 50] This mode was observed in experiments even when defects

are introduced (Fig. 5 b-d). The other higher-order S modes are modes not uniformly excited (Fig. 5e-k) and have characters more consistent with quadrupoles (Q_1 and Q_2), but those high-order symmetric modes are not observed in the experiments. This is most likely due to the in-coupling depending upon the net polarization of the pillars along the wavefront of the incident field, therefore in-coupling to the non-M S and A modes is reduced in comparison to the M mode. The A modes we observed are the first type of the A modes (type I) as the out-of-plane field switches polarity across one of the central planes of the subarray, with these modes illustrated in panels l-q of Figure 5. There are also type II A modes where the out-of-plane field switches polarity across both resonator array's central planes, which are illustrated in Fig. S7. Note that the behavior of each type of A mode is similar. Regardless of whether they are of type I or type II symmetry each has zero net charge on the pillar end facets, meaning they do not couple strongly to the propagating SPhPs supported on the substrate surface. As for the type I A mode illustrating in Fig. 5l-o, only the left and right edges in the unit cell exhibit strong field confinement featuring opposite phase, leaving the middle pillars with a minimal electric field magnitude. A second A mode emerges for the square 3x3 (Fig. 3p) and 3x3 without center pillar structure (Fig. 5q), yet only the mode in the 3x3 structure without the center pillar is observed in our experimental data. This is probably because the three central pillars screen the array dipole moment. Therefore, removing the central pillar breaks the symmetry, enabling it to couple to free space. These calculated field profiles demonstrate the intrinsic role that symmetry plays in the resultant collectively excited LSPhP modes and dispersion.

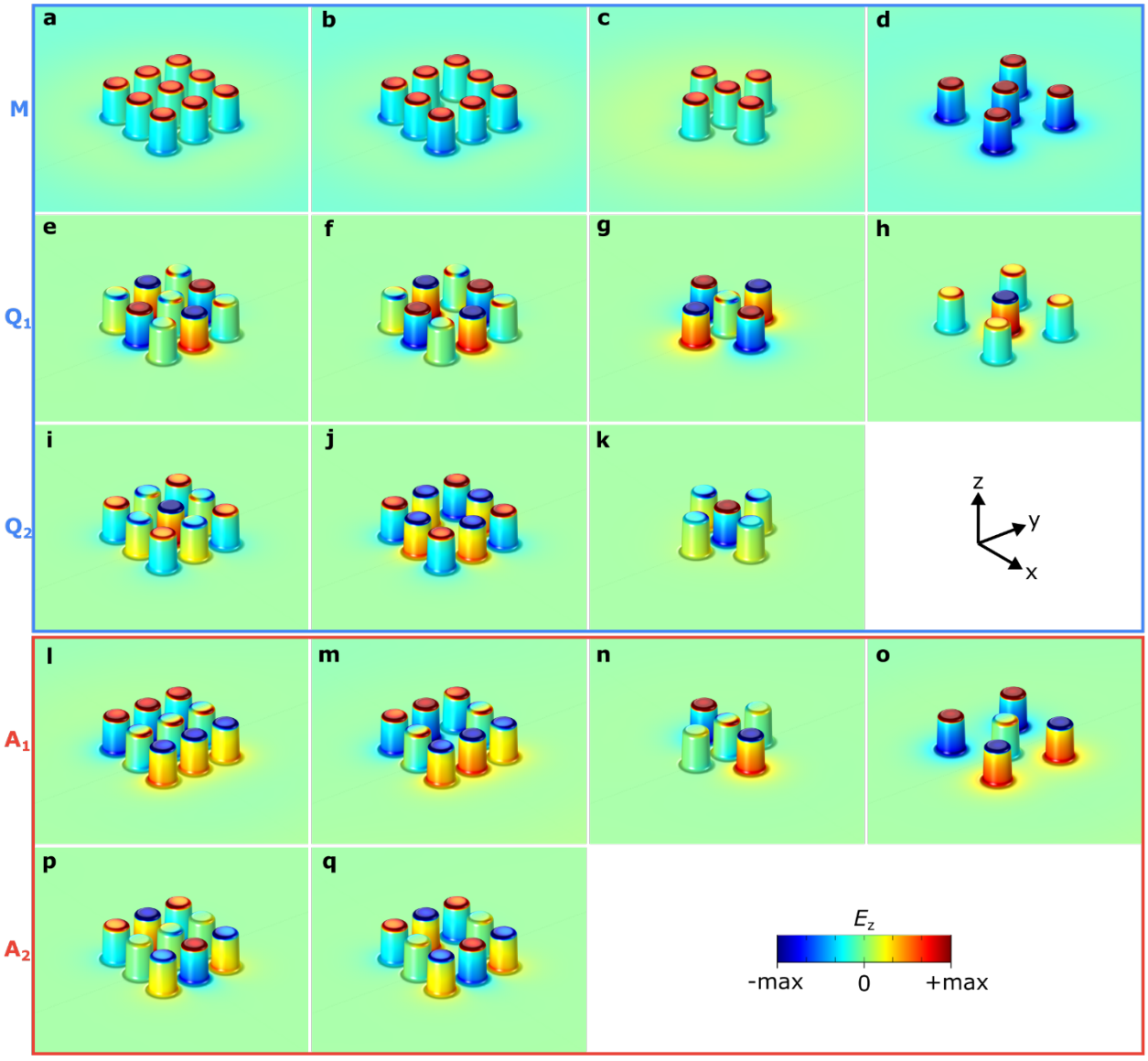

Figure 5: Field profiles of the symmetric and anti-symmetric modes in the complex unit cell. Calculated fields (E_z) of the symmetric mode with uniform excitation (M) for the square 3x3 structure (a), 3x3 structure without center pillar (b), 3x3 structure features as cross-shape (c), 3x3 structure features as X-shape (d). Simulated fields (E_z) of the second symmetric mode (Q_1) for the square 3x3 structure (e), 3x3 structure without center pillar (f), 3x3 structure features as cross-shape (g), 3x3 structure features as X-shape (h). Calculated fields (E_z) of the third symmetric mode (Q_2) for the square 3x3 structure (i), 3x3 structure without center pillar (j), 3x3 structure features as cross-shape (k). Calculated fields (E_z) of the first anti-symmetric mode (A_1) for the square 3x3 structure (l), 3x3 structure without center pillar (m), 3x3 structure features as cross-shape (n), 3x3 structure features as X-shape (o). Calculated fields (E_z) of the second anti-symmetric mode (A_2) for the square 3x3 structure (p), 3x3 structure without center pillar (q).

Conclusion

In this work, we demonstrated subarray designs of subwavelength nanopillars to support collective low-loss, subdiffractional LSPhPs modes, enabling the roughly independent design of the near-field patterns and far-field resonance condition. Within these results we provided experimental evidence of phonon polaritons splitting into S and A modes when a subarray is formed. By exploring the gap, diameter and unit cell size dependences, as well as the influence of local defects within the subarray structure, we were

able to demonstrate that the dispersion of the monopolar-like resonances remains similar for all structures, despite significant modifications to the underlying field profiles. Moreover, the collectively excited modes are robust even to defects introduced into the unit cell and the symmetry inside the unit cell plays a role in the light confinement. Future studies to investigate the near-field response of these collective modes *via* nano-FTIR and/or s-SNOM techniques promise to be specifically valuable.[55] Additionally, the role of symmetry breaking in the unit cell promises to be an additional fruitful direction. Our work represents complex hierarchical phonon polaritonic near-field design with the tailored responses for a wide range of IR applications such as surface-enhanced spectroscopy and IR barcoding or nanophotonic narrow-band thermal emitters.

Methods

Device fabrication

All the SiC nanopillar arrays (100 μm x 100 μm array size) are fabricated into semi-insulating 4H-SiC substrates using standard electron beam lithography (EBL) process. A 250 nm PMMA 950 A4 layer was spin-coated at 3000 rpm followed by deposition of 10 nm-thick chromium as the conduction layer using thermal evaporation. The patterns were then defined using EBL followed by depositing 100 nm-thick Nickel as a dry etch mask using electron beam evaporation. The SiC nanopillars were etched using reactive ion etching (RIE) using a mixture of O_2 and SF_6 at an etching rate of 375 nm/min, and all the nanopillar structures are etched to 1 μm.

Optical characterization

The room-temperature reflection spectra for the fabricated samples are collected using a Hyperion 2000 IR microscope attached to a Bruker Vertex 70v Fourier transform infrared (FTIR) spectrometer with a liquid-nitrogen-cooled HgCdTe (MCT) detector. The microscope objective used is a 36× Cassegrain objective (Pike Technologies), which illuminates the sample along the array axis with an average incident angle of 25°.

Numerical simulations

Finite element method (FEM) simulations were performed in CST studio suite 2018 using the structure mentioned in the main text. The unit cell boundary conditions and a perfectly matched layer for the substrate are used in the simulations. The dielectric function used for 4H-SiC was derived from that presented in Ref [56].

Tight-binding theoretical model

The eigenmodes of a single, isolated nanopillar on same-material substrate satisfy the electromagnetic wave equation

$$\nabla \times \nabla \times \mathrm{E}_1 = \epsilon_0(\mathrm{r}) \frac{\omega_1^2}{\mathrm{c}^2} \mathrm{E}_1,$$

where E_1 is the electric field, ϵ_0 is the dielectric function of the single-resonator on substrate system and ω_1 is the mode frequency. As discussed in the main text single nanopillar system supports a single, bright, out-of-plane polarized mode termed the monopole, or M mode. The M mode extends over the substrate, allowing for long-range interactions between adjacent nanopillars.

In an isolated subarray, comprised of a finite array of nanopillars on substrate the M modes of closely spaced pillars interact forming new eigenmodes which are linear superpositions of the M modes of the individual nanopillars. These modes satisfy the electromagnetic wave equation

$$\nabla \times \nabla \times \mathbf{E}_{\mathrm{i}} = \epsilon_1(\mathbf{r}) \frac{\omega_{\mathrm{i}}^2}{c^2} \mathbf{E}_{\mathrm{i}},$$

where $\boldsymbol{E_i}$ is the electric field, ω_i is the mode frequency and ϵ_1 is the dielectric function of the sub-array system, which differs from ϵ_0 in Eq. 1 as it accounts for more than one pillar. As shown in Fig. 5 this leads to modes which are linear superpositions of the M modes. This can be understood in the context of a tight-binding hybridization model, where each pillar couples with the other pillars comprising the subarray. For an $N \times N$ subarray this leads to N^2, possibly degenerate modes. The modal composition can be qualitatively understood considering the Hamiltonian problem

$$\widehat{\mathcal{H}} x_i = \hbar \omega_i x_i,$$

where $\widehat{\mathcal{H}}$ is the Hamiltonian containing the bare mode energies and interpillar couplings and x_i is the vector of modal amplitudes within each pillar. Considering only nearest neighbor couplings this leads to one eigenmode where all pillars have the same polarization (the M mode) and $N^2 - 1$ other eigenmodes.

Going forward we consider the electric field to be real and normalized to unity

$$\int d^3r \, \epsilon_i(r) E_i \cdot E_i = 1.$$

The eigenmodes of the infinite square lattice of sub-arrays studied in this work satisfy electromagnetic wave equation

$$\nabla \times \nabla \times E_{k_\parallel,i} = \epsilon(r) \frac{\omega_{k_\parallel,i}^2}{c^2} E_{k_\parallel,i},$$

where ϵ is the dielectric function of the infinite system with contribution ϵ_1 in each unit cell and $k_\parallel$ labels the wavevector component parallel to the substrate. In the periodic system the solution is a Bloch wave, which is just a linear superposition of the modes in each sub-array, labelled n

$$E_{k_\parallel,i}(r,t) = E_0 e^{i\omega_{k_\parallel,i} t} \sum_{m,n} e^{-ik_\parallel \cdot (m\hat{x}+n\hat{y})R} E_i(r - (m\hat{x}+n\hat{y})R).$$

where R is the array period. Substituting this into the full-system wave-equation yields the dispersion relation

$$\omega_{k_\parallel,i}^2 = \omega_i^2 \frac{1 + \sum_{mn\neq 0} e^{-ik_\parallel (m\hat{x}+n\hat{y})R} \beta_{mn,i}}{1 + \Delta\eta_i + \sum_{mn\neq 0} e^{-ik_\parallel (m\hat{x}+n\hat{y})R} \eta_{mn,i}}.$$

where the Greek letters represent overlap integrals between the resonator labelled 00 and that at mn and are given by

$$\Delta\eta_i = \int d^3r \, [\epsilon(r) - \epsilon_1(r)] E_i(r) \cdot E_i(r),$$

$$\eta_{mn,i} = \int d^3r\, \epsilon(r) E_i(r) \cdot E_i(r - [m\hat{x} + n\hat{y}]R),$$

$$\beta_{mn,i} = \int d^3r\, \epsilon_1(r - [m\hat{x} + n\hat{y}]R) E_i(r) \cdot E_i(r - [m\hat{x} + n\hat{y}]R).$$

In the limit of nearest-neighbor coupling between adjacent subarrays, small inter-array coupling in comparison to the bare mode frequency, and equal coupling to subarrays along each axis we find for small in-plane wavevector

$$\omega_{k_\parallel,i} \approx \omega_i \left[1 + 2\left(\beta_{01,i} - \eta_{01,i} - \frac{\Delta\eta_i}{2}\right)\right].$$

The $\Delta\eta_i$ term represents a self-interaction. Other terms arise from interactions between adjacent sub-arrays. As illustrated in Fig. 5, only the bright mode of the subarray, where all the individual pillars are polarized in the same direction, extends far across the substrate. As the signs of the interacting fields are equal, and the dielectric function of the resonators is large and negative in the Reststrahlen region, this leads to a repulsive blue shift in mode frequency for these modes. The non-symmetric modes only interact weakly as they are confined to the individual subarrays, as illustrated in Fig. 5.

Eigenmodes calculations

The eigenmodes of the individual nanopillar subarrays (Fig. 5) are calculated utilizing the modal analysis tool QNMEig, which allows for the calculation of the quasi-normal modes of open photonic systems [57].

Acknowledgements

Funding for G.L. was provided through an STTR program provided by the National Science Foundation, Division of Industrial Innovation and Partnerships (IIP) (Award No. 2014798). A portion of this research was conducted at the Vanderbilt Institute of Nanoscale Science and Engineering. S.D.L. was supported by a Royal Society Research fellowship (Grant no. URF\R\180002), and the Philip Leverhulme prize. C.R.G. was supported by the Royal Society (Grant no. RGF\EA\181001), and a Research Grant of the Leverhulme Trust (Grant No. RPG-2019-174). J.R.N and J.D.C. were supported by Office of Naval Research Grant N00014-18-12107. Research at the Naval Research Laboratory was supported by the Office of Naval Research. A portion of this research was conducted at the Center for Nanophase Materials Sciences, which is a DOE Office of Science User Facility.

Supporting Information

The supporting information is available at xxx.

Fabricated subarrays; polarization properties of the collectively excited LSPhP modes; collectively excited LSPhP modes at normal incidence; the coupling between the anti-symmetric mode and the ZFLO mode; angular dispersion of the collectively excited LSPhP modes, field profiles of the symmetric and anti-symmetric modes in the square unit cells, and two types of anti-symmetric modes.

References

1. Autore, M.; Dolado, I.; Li, P.; Esteban, R.; Alfaro‐Mozaz, F. J.; Atxabal, A.; Liu, S.; Edgar, J. H.; Vélez, S.; Casanova, F.; Hueso, L. E.; Aizpurua, J.; Hillenbrand, R., Enhanced Light–Matter Interaction in 10B Monoisotopic Boron Nitride Infrared Nanoresonators. *Advanced Optical Materials* **2020**.
2. Razdolski, I.; Chen, Y.; Giles, A. J.; Gewinner, S.; Schollkopf, W.; Hong, M.; Wolf, M.; Giannini, V.; Caldwell, J. D.; Maier, S. A.; Paarmann, A., Resonant Enhancement of Second-Harmonic Generation in the Mid-Infrared Using Localized Surface Phonon Polaritons in Subdiffractional Nanostructures. *Nano Lett* **2016,** *16* (11), 6954-6959.
3. Wang, T.; Li, P.; Chigrin, D. N.; Giles, A. J.; Bezares, F. J.; Glembocki, O. J.; Caldwell, J. D.; Taubner, T., Phonon-Polaritonic Bowtie Nanoantennas: Controlling Infrared Thermal Radiation at the Nanoscale. *ACS Photonics* **2017,** *4* (7), 1753-1760.
4. Miller, D. A. B., Attojoule Optoelectronics for Low-Energy Information Processing and Communications. *J. Lightwave Technol.* **2017,** *35* (3), 346-396.
5. Caldwell, J. D.; Lindsay, L.; Giannini, V.; Vurgaftman, I.; Reinecke, T. L.; Maier, S. A.; Glembocki, O. J., Low-loss, infrared and terahertz nanophotonics using surface phonon polaritons. *Nanophotonics* **2015,** *4* (1), 44-68.
6. Foteinopoulou, S.; Devarapu, G. C. R.; Subramania, G. S.; Krishna, S.; Wasserman, D., Phonon-polaritonics: enabling powerful capabilities for infrared photonics. *Nanophotonics* **2019,** *8* (12), 2129-2175.
7. Folland, T. G.; Nordin, L.; Wasserman, D.; Caldwell, J. D., Probing polaritons in the mid- to far-infrared. *J. Appl. Phys.* **2019,** *125* (19), 191102.
8. Adachi, S., *Handbook on Physical Properties of Semiconductors*. Kluwer Academic Publishers: Boston, 2004; p 1-344.
9. Caldwell, J. D.; Glembocki, O. J.; Francescato, Y.; Sharac, N.; Giannini, V.; Bezares, F. J.; Long, J. P.; Owrutsky, J. C.; Vurgaftman, I.; Tischler, J. G.; Wheeler, V. D.; Bassim, N. D.; Shirey, L. M.; Kasica, R.; Maier, S. A., Low-loss, extreme subdiffraction photon confinement via silicon carbide localized surface phonon polariton resonators. *Nano Lett* **2013,** *13* (8), 3690-3697.
10. Caldwell, J. D.; Kretinin, A. V.; Chen, Y.; Giannini, V.; Fogler, M. M.; Francescato, Y.; Ellis, C. T.; Tischler, J. G.; Woods, C. R.; Giles, A. J.; Hong, M.; Watanabe, K.; Taniguchi, T.; Maier, S. A.; Novoselov, K. S., Sub-diffractional volume-confined polaritons in the natural hyperbolic material hexagonal boron nitride. *Nat Commun* **2014,** *5*, 5221.
11. Chen, Y.; Francescato, Y.; Caldwell, J. D.; Giannini, V.; Maß, T. W. W.; Glembocki, O. J.; Bezares, F. J.; Taubner, T.; Kasica, R.; Hong, M.; Maier, S. A., Spectral Tuning of Localized Surface Phonon Polariton Resonators for Low-Loss Mid-IR Applications. *ACS Photonics* **2014,** *1* (8), 718-724.
12. Ellis, C. T.; Tischler, J. G.; Glembocki, O. J.; Bezares, F. J.; Giles, A. J.; Kasica, R.; Shirey, L.; Owrutsky, J. C.; Chigrin, D. N.; Caldwell, J. D., Aspect-ratio driven evolution of high-order resonant modes and near-field distributions in localized surface phonon polariton nanostructures. *Sci Rep* **2016,** *6*, 32959.
13. Wang, T.; Li, P.; Hauer, B.; Chigrin, D. N.; Taubner, T., Optical properties of single infrared resonant circular microcavities for surface phonon polaritons. *Nano Lett* **2013,** *13* (11), 5051-5.
14. Spann, B. T.; Compton, R.; Ratchford, D.; Long, J. P.; Dunkelberger, A. D.; Klein, P. B.; Giles, A. J.; Caldwell, J. D.; Owrutsky, J. C., Photoinduced tunability of the reststrahlen band in4H−SiC. *Physical Review B* **2016,** *93* (8).
15. Dunkelberger, A. D.; Ellis, C. T.; Ratchford, D. C.; Giles, A. J.; Kim, M.; Kim, C. S.; Spann, B. T.; Vurgaftman, I.; Tischler, J. G.; Long, J. P.; Glembocki, O. J.; Owrutsky, J. C.; Caldwell, J. D., Active tuning of surface phonon polariton resonances via carrier photoinjection. *Nature Photonics* **2017,** *12* (1), 50-56.
16. Yoo, D.; de Leon-Perez, F.; Pelton, M.; Lee, I. H.; Mohr, D. A.; Raschke, M. B.; Caldwell, J. D.; Martin-Moreno, L.; Oh, S. H., Ultrastrong plasmon-phonon coupling via epsilon-near-zero nanocavities. *Nature Photonics* **2020**.

17. Runnerstrom, E. L.; Kelley, K. P.; Folland, T. G.; Nolen, J. R.; Engheta, N.; Caldwell, J. D.; Maria, J. P., Polaritonic Hybrid-Epsilon-near-Zero Modes: Beating the Plasmonic Confinement vs Propagation-Length Trade-Off with Doped Cadmium Oxide Bilayers. *Nano Lett* **2019,** *19* (2), 948-957.
18. Passler, N. C.; Gubbin, C. R.; Folland, T. G.; Razdolski, I.; Katzer, D. S.; Storm, D. F.; Wolf, M.; De Liberato, S.; Caldwell, J. D.; Paarmann, A., Strong Coupling of Epsilon-Near-Zero Phonon Polaritons in Polar Dielectric Heterostructures. *Nano Lett* **2018,** *18* (7), 4285-4292.
19. Woessner, A.; Lundeberg, M. B.; Gao, Y.; Principi, A.; Alonso-Gonzalez, P.; Carrega, M.; Watanabe, K.; Taniguchi, T.; Vignale, G.; Polini, M.; Hone, J.; Hillenbrand, R.; Koppens, F. H., Highly confined low-loss plasmons in graphene-boron nitride heterostructures. *Nat Mater* **2015,** *14* (4), 421-5.
20. Brar, V. W.; Jang, M. S.; Sherrott, M.; Kim, S.; Lopez, J. J.; Kim, L. B.; Choi, M.; Atwater, H., Hybrid surface-phonon-plasmon polariton modes in graphene/monolayer h-BN heterostructures. *Nano Lett* **2014,** *14* (7), 3876-80.
21. Dai, S.; Ma, Q.; Liu, M. K.; Andersen, T.; Fei, Z.; Goldflam, M. D.; Wagner, M.; Watanabe, K.; Taniguchi, T.; Thiemens, M.; Keilmann, F.; Janssen, G. C.; Zhu, S. E.; Jarillo-Herrero, P.; Fogler, M. M.; Basov, D. N., Graphene on hexagonal boron nitride as a tunable hyperbolic metamaterial. *Nat Nanotechnol* **2015,** *10* (8), 682-6.
22. Rivera, N.; Christensen, T.; Narang, P., Phonon Polaritonics in Two-Dimensional Materials. *Nano Lett* **2019,** *19* (4), 2653-2660.
23. Zhang, Q.; Hu, G.; Ma, W.; Li, P.; Krasnok, A.; Hillenbrand, R.; Alù, A.; Qiu, C.-W., Interface nano-optics with van der Waals polaritons. *Nature* **2021,** *597* (7875), 187-195.
24. Zhang, Q.; Ou, Q.; Hu, G.; Liu, J.; Dai, Z.; Fuhrer, M. S.; Bao, Q.; Qiu, C. W., Hybridized Hyperbolic Surface Phonon Polaritons at alpha-MoO3 and Polar Dielectric Interfaces. *Nano Lett* **2021**.
25. Gubbin, C. R.; Martini, F.; Politi, A.; Maier, S. A.; De Liberato, S., Strong and Coherent Coupling between Localized and Propagating Phonon Polaritons. *Phys. Rev. Lett.* **2016,** *116* (24), 246402.
26. Gubbin, C. R.; Berte, R.; Meeker, M. A.; Giles, A. J.; Ellis, C. T.; Tischler, J. G.; Wheeler, V. D.; Maier, S. A.; Caldwell, J. D.; De Liberato, S., Hybrid longitudinal-transverse phonon polaritons. *Nat Commun* **2019,** *10* (1), 1682.
27. Lu, G.; Gubbin, C. R.; Nolen, J. R.; Folland, T.; Tadjer, M. J.; De Liberato, S.; Caldwell, J. D., Engineering the Spectral and Spatial Dispersion of Thermal Emission via Polariton-Phonon Strong Coupling. *Nano Lett* **2021,** *21* (4), 1831-1838.
28. Autore, M.; Li, P.; Dolado, I.; Alfaro-Mozaz, F. J.; Esteban, R.; Atxabal, A.; Casanova, F.; Hueso, L. E.; Alonso-Gonzalez, P.; Aizpurua, J.; Nikitin, A. Y.; Velez, S.; Hillenbrand, R., Boron nitride nanoresonators for phonon-enhanced molecular vibrational spectroscopy at the strong coupling limit. *Light Sci Appl* **2018,** *7*, 17172.
29. Li, K.; Fitzgerald, J. M.; Xiao, X.; Caldwell, J. D.; Zhang, C.; Maier, S. A.; Li, X.; Giannini, V., Graphene Plasmon Cavities Made with Silicon Carbide. *ACS Omega* **2017,** *2* (7), 3640-3646.
30. Wan, W.; Yang, X.; Gao, J., Strong coupling between mid-infrared localized plasmons and phonons. *Opt Express* **2016,** *24* (11), 12367-74.
31. Razdolski, I.; Passler, N. C.; Gubbin, C. R.; Winta, C. J.; Cernansky, R.; Martini, F.; Politi, A.; Maier, S. A.; Wolf, M.; Paarmann, A.; De Liberato, S., Second harmonic generation from strongly coupled localized and propagating phonon-polariton modes. *Physical Review B* **2018,** *98* (12).
32. Berte, R.; Gubbin, C. R.; Wheeler, V. D.; Giles, A. J.; Giannini, V.; Maier, S. A.; De Liberato, S.; Caldwell, J. D., Sub-nanometer Thin Oxide Film Sensing with Localized Surface Phonon Polaritons. *ACS Photonics* **2018,** *5* (7), 2807-2815.
33. Feng, K.; Streyer, W.; Islam, S. M.; Verma, J.; Jena, D.; Wasserman, D.; Hoffman, A. J., Localized surface phonon polariton resonances in polar gallium nitride. *Appl. Phys. Lett.* **2015,** *107* (8).
34. Halas, N. J.; Lal, S.; Chang, W. S.; Link, S.; Nordlander, P., Plasmons in strongly coupled metallic nanostructures. *Chem. Rev.* **2011,** *111* (6), 3913-61.

35. Prodan, E.; Radloff, C.; Halas, N. J.; Nordlander, P., A hybridization model for the plasmon response of complex nanostructures. *Science* **2003,** *302* (5644), 419-22.
36. Jain, P. K.; Huang, W.; El-Sayed, M. A., On the Universal Scaling Behavior of the Distance Decay of Plasmon Coupling in Metal Nanoparticle Pairs: A Plasmon Ruler Equation. *Nano Letters* **2007,** *7* (7), 2080-2088.
37. Rechberger, W.; Hohenau, A.; Leitner, A.; Krenn, J. R.; Lamprecht, B.; Aussenegg, F. R., Optical properties of two interacting gold nanoparticles. *Opt. Commun.* **2003,** *220* (1-3), 137-141.
38. Grigorenko, A. N.; Geim, A. K.; Gleeson, H. F.; Zhang, Y.; Firsov, A. A.; Khrushchev, I. Y.; Petrovic, J., Nanofabricated media with negative permeability at visible frequencies. *Nature* **2005,** *438* (7066), 335-8.
39. Brandl, D. W.; Mirin, N. A.; Nordlander, P., Plasmon modes of nanosphere trimers and quadrumers. *J Phys Chem B* **2006,** *110* (25), 12302-10.
40. Fan, J. A.; Bao, K.; Wu, C.; Bao, J.; Bardhan, R.; Halas, N. J.; Manoharan, V. N.; Shvets, G.; Nordlander, P.; Capasso, F., Fano-like interference in self-assembled plasmonic quadrumer clusters. *Nano Lett* **2010,** *10* (11), 4680-5.
41. Hentschel, M.; Saliba, M.; Vogelgesang, R.; Giessen, H.; Alivisatos, A. P.; Liu, N., Transition from isolated to collective modes in plasmonic oligomers. *Nano Lett* **2010,** *10* (7), 2721-6.
42. Hentschel, M.; Dregely, D.; Vogelgesang, R.; Giessen, H.; Liu, N., Plasmonic oligomers: the role of individual particles in collective behavior. *ACS Nano* **2011,** *5* (3), 2042-50.
43. Lassiter, J. B.; Sobhani, H.; Knight, M. W.; Mielczarek, W. S.; Nordlander, P.; Halas, N. J., Designing and deconstructing the Fano lineshape in plasmonic nanoclusters. *Nano Lett* **2012,** *12* (2), 1058-62.
44. Rahmani, M.; Lei, D. Y.; Giannini, V.; Lukiyanchuk, B.; Ranjbar, M.; Liew, T. Y.; Hong, M.; Maier, S. A., Subgroup decomposition of plasmonic resonances in hybrid oligomers: modeling the resonance lineshape. *Nano Lett* **2012,** *12* (4), 2101-6.
45. Bautista, G.; Dreser, C.; Zang, X.; Kern, D. P.; Kauranen, M.; Fleischer, M., Collective Effects in Second-Harmonic Generation from Plasmonic Oligomers. *Nano Lett* **2018,** *18* (4), 2571-2580.
46. Lu, G.; Tadjer, M.; Caldwell, J. D.; Folland, T. G., Multi-frequency coherent emission from superstructure thermal emitters. *Appl. Phys. Lett.* **2021,** *118* (14).
47. Kravets, V. G.; Kabashin, A. V.; Barnes, W. L.; Grigorenko, A. N., Plasmonic Surface Lattice Resonances: A Review of Properties and Applications. *Chem. Rev.* **2018,** *118* (12), 5912-5951.
48. Greffet, J. J.; Carminati, R.; Joulain, K.; Mulet, J. P.; Mainguy, S.; Chen, Y., Coherent emission of light by thermal sources. *Nature* **2002,** *416* (6876), 61-64.
49. Çetin, A. E.; Yanik, A. A.; Yilmaz, C.; Somu, S.; Busnaina, A.; Altug, H., Monopole antenna arrays for optical trapping, spectroscopy, and sensing. *Appl. Phys. Lett.* **2011,** *98* (11).
50. Gubbin, C. R.; Maier, S. A.; De Liberato, S., Theoretical investigation of phonon polaritons in SiC micropillar resonators. *Physical Review B* **2017,** *95* (3).
51. Lu, G.; Nolen, J. R.; Folland, T. G.; Tadjer, M. J.; Walker, D. G.; Caldwell, J. D., Narrowband Polaritonic Thermal Emitters Driven by Waste Heat. *ACS Omega* **2020,** *5* (19), 10900-10908.
52. Nakashima, S.; Harima, H., Raman Investigation of SiC Polytypes. *physica status solidi (a)* **1997,** *162* (1), 39-64.
53. Nordlander, P.; Oubre, C.; Prodan, E.; Li, K.; Stockman, M. I., Plasmon Hybridization in Nanoparticle Dimers. *Nano Letters* **2004,** *4* (5), 899-903.
54. Lee, I. H.; He, M.; Zhang, X.; Luo, Y.; Liu, S.; Edgar, J. H.; Wang, K.; Avouris, P.; Low, T.; Caldwell, J. D.; Oh, S. H., Image polaritons in boron nitride for extreme polariton confinement with low losses. *Nat Commun* **2020,** *11* (1), 3649.
55. Mancini, A.; Gubbin, C. R.; Berte, R.; Martini, F.; Politi, A.; Cortes, E.; Li, Y.; De Liberato, S.; Maier, S. A., Near-Field Spectroscopy of Cylindrical Phonon-Polariton Antennas. *ACS Nano* **2020**.

56. Paarmann, A.; Razdolski, I.; Gewinner, S.; Schöllkopf, W.; Wolf, M., Effects of crystal anisotropy on optical phonon resonances in midinfrared second harmonic response of SiC. *Physical Review B* **2016,** *94* (13), 134312.
57. Yan, W.; Faggiani, R.; Lalanne, P., Rigorous modal analysis of plasmonic nanoresonators. *Physical Review B* **2018,** *97* (20).

For Table of Contents Only